ELSEVIER

NMR spin relaxation methods for characterization of disorder and folding in proteins

Clay Bracken

Department of Biochemistry, Weill Medical College of Cornell University, New York, NY 10021, USA

The flexibility and dynamics of proteins directly influence the processes of protein folding, recognition, and function. NMR spin relaxation methods are used to assess the dynamics and mobility of proteins, for fast ps and ns motions as well as slower μs and ms events. The degree of protein flexibility and disorder as well as the changes in protein flexibility can be assessed by NMR spin relaxation methods at individual residues within the protein. In addition to probing protein dynamics, the changes in the NMR-derived order parameters can be used to estimate the entropic contributions of order–disorder transitions. Furthermore, kinetic processes in the ms time regime may be directly investigated to extract the rates of conformational interconversion, ligand binding, and protein folding processes. We show how a variety of dynamical information can be obtained from NMR relaxation measurements. We present examples that illustrate the use of NMR spin relaxation analysis for investigation of folding and disorder in proteins.

INTRODUCTION

The absence of stable secondary and tertiary structure in proteins was once viewed as the absence of biological function. However, a number of globally disordered yet biologically active peptides and proteins have been characterized recently, suggesting that dynamics in proteins may significantly influence a number of biological processes (for a review see Wright and Dyson).[1] Disorder in proteins can confer significant advantages in certain biological processes. First, the degree of flexibility in a protein recognition or binding region will have an impact on the thermodynamics of protein association through the entropic cost paid for ordering the protein backbone and sidechains. Second, disordered regions allow variability in protein recognition motifs, permitting a given sequence to adaptively recognize multiple binding partners. Third, flexible regions in proteins offer important handles for modulating the in-vivo lifetime of proteins through proteolytic degradation. Finally, a complete understanding of unfolded protein states is necessary for elucidating the protein folding process since any preexisting structural propensities may positively or negatively impact both protein folding rates and protein stability.

Solution NMR spectroscopy is the most powerful biophysical technique for characterizing disordered states of proteins, assessing the degree of protein flexibility, and elucidating the mechanism of protein folding. The utility of NMR for assessing protein flexibility and disorder is a direct result of the development of multidimensional homonuclear and heteronuclear NMR methods for resolving and assigning individual resonances frequencies to specific locations within the amino-acid sequence.[2] This allows the properties of the individual nuclei to be monitored at known sites within the protein and serve as reporters of both structural and dynamical information.

A wide variety of solution NMR methods (See Table 1) have been developed for analyzing residue-specific information on disordered proteins and peptides. Of the available techniques one of the most informative for characterizing protein flexibility is NMR spin relaxation analysis.[3–5] The relaxation rates of nuclei are directly tied to the motional properties of the molecule, therefore differences in nuclear relaxation rates are related to motional differences within a molecule. Here we give an overview of ^{13}C and ^{15}N relaxation methods for characterizing the motional properties of proteins with specific examples assessing protein flexibility and characterizing equilibrium protein folding through the application of heteronuclear relaxation methods.

Relaxation of ^{13}C and ^{15}N nuclei

The relaxation of nuclear spins to a statistical equilibrium state occurs primarily through the coupling of the nuclear spin transitions to the surroundings termed the "lattice."[6]. In solution changes in motions on the ps to ns time scale result in

Corresponding author: C. Bracken, Department of Biochemistry, Weill Medical College of Cornell University, New York, NY 10021, USA. Tel.: 212-746-6473; fax: 212-746-8329.

E-mail address: wcb2001@med.cornell.edu

Journal of Molecular Graphics and Modelling 19, 3–12, 2001

655 Avenue of the Americas, New York, NY 10010

1093-3263/01/$–see front matter
PII S1093-3263(00)00136-4

Table 1. NMR spectroscopic techniques for characterizing protein structure and flexibility

NMR Observable	Applications	Comments
Nuclear Overhauser effect (NOE)	Secondary and Tertiary Structure Determination	Primary NMR method for generating long range distance constraints.
Relaxation Measurements	Flexibility and Motion	Measurement of global and local correlation times, order parameters, chemical exchange.
Chemical Shifts	Secondary Structure Characterization	Backbone chemical shifts are often correlated to the protein secondary structure.
Hydrogen Exchange	Protein stability Hydrogen bonding	Measurement of protection rates in protein folding.
Dipolar Couplings	Structural characterization	Orientational information, local order parameters.
Diffusion Measurements	Hydrodynamic characterization	Global shape information can distinguish folded and unfolded structures.
Paramagnetic Probes	Solvent binding and protein accessibility	Distance constraints in proteins by paramagnetic broadening.
Scalar couplings	Secondary structure	Information about bond torsion angles.

observable changes in nuclear spin relaxation rates. Additionally, motions on the ms to μs time scale may be detected through chemical exchange between two or more distinct chemical environments. By monitoring the relaxation rates at specific resonances, details of the motional dynamics within proteins can be assessed. A variety of heteronuclear relaxation experiments now exist to monitor ^{1}H, ^{2}H, ^{13}C, and ^{15}N nuclei allowing access to motional information at multiple locations within the protein backbone and sidechain.[3–5] We will focus on selectively labeled $^{13}C^{\alpha}$ and ^{15}N relaxation of the backbone resonances.

The most commonly employed NMR relaxation experiments monitor the ^{15}N amide resonances of the protein backbone. The advantages of ^{15}N relaxation measurements for the study of proteins are the low cost of the ^{15}N isotope, the absence of complex scalar homonuclear and heteronuclear couplings, the absence of significant remote interactions with neighboring spins, and the superior resolution of the $^{1}H^{N}$ and ^{15}N dimensions. In addition, the interpretation and methodology for application of ^{15}N spin relaxation experiments to proteins is well established.[7,8] In contrast, the applications and theory for characterizing protein dynamics from ^{13}C nuclear spin relaxation are not as well established or widely applied as ^{15}N spectroscopic methods[3,4]. However, ^{13}C NMR spectroscopy is particularly well-suited for investigation of conformational dynamics of unstructured proteins or in cases were NMR dynamics are used to monitor equilibrium protein folding processes.

Protein relaxation analysis using ^{13}C has a number of demonstrated advantages. In proteins and peptides selectively enriched at specific site with ^{13}C via peptide synthesis or selective labeling strategies, the complications encountered from ^{13}C–^{13}C scalar and dipolar couplings in uniformly ^{13}C-labeled samples are avoided. Unlike the amide protons, in ^{13}C the attached protons are stable, preventing fast exchange with solvent in unfolded or partially folded proteins that can reduce the sensitivity of ^{15}N NMR spectroscopy and limits the range of experimental conditions employed. A significant advantage of using the alpha and carbonyl backbone carbons for relaxation studies is that the chemical shifts are diagnostic of secondary structural preferences, making the results more easily interpretable.[9]

Established NMR pulse sequences now exist for collecting longitudinal relaxation rates (R_1), transverse relaxation rates (R_2), and heteronuclear NOE data in labeled proteins and peptides.[7,8] The most widely applied pulse sequences utilize two dimensional heteronuclear correlation spectra to allow observation of the relaxation effects of the given nucleus indirectly through the attached proton. In solution, the relaxation rates of the isolated ^{1}H-^{15}N and ^{1}H-$^{13}C^{\alpha}$ heteronuclear atoms are dominated by the dipolar interaction with the attached proton and by the chemical shift anisotropy interaction.[6] For the amide ^{1}H-^{15}N and selectively labeled ^{1}H-$^{13}C^{\alpha}$ of the peptide backbone, the relaxation rates are given:

$$R_1 = (d^2/4)[3J(\omega_X) + 6J(\omega_H + \omega_X) + J(\omega_H - \omega_X)] + c^2 J(\omega_X) \quad (1)$$

$$R_2 = (d^2/8)[4J(0) + 3J(\omega_X) + J(\omega_H - \omega_X) + 6J(\omega_H + \omega_X)] + (c^2/6)[4J(0) + 3J(\omega_X)] + \Delta R_2(1/\tau_{cp}) \quad (2)$$

$$NOE = 1 + (d^2/4R_1)(\gamma_H/\gamma_X)[6J(\omega_H + \omega_X) - J(\omega_H - \omega_X)], \quad (3)$$

where $d(\mu_0 h \gamma_H \gamma_X / 8\pi^2)\langle r_{XH}^{-3}\rangle$, $c = \omega_X \Delta\sigma/\sqrt{3}$, μ_0 is the permeability of free space, h is Planck's constant, γ_H is the gyromagnetic ratio of ^{1}H, γ_X is the gyromagnetic ratio of the X nucleus (either ^{13}C or ^{15}N), r_{XH} is the average bond length (r_{CH} =1.09 Å and r_{NH} = 1.02 Å), $\Delta\sigma$ is the chemical shift anisotropy ($\Delta\sigma$ = 25 ppm for $^{13}C^{\alpha}$ and $\Delta\sigma$ = 160 ppm for ^{15}N), $\Delta R_2(1/\tau_{cp})$ is the residual chemical exchange term that accounts for conformational exchange processes that perturb the chemical shift on the ms to μs timescale and contribute to the observed R_2 rate constant during the Carr-Purcell-Meiboom-Gill (CPMG) sequence used during the R_2 relaxation period, and J(ω) is the power spectral density function.

The power spectral density function, J(ω), defines the frequency spectrum of overall and intramolecular motions that reorient the X—H bond. The power spectral density function describes the available energy density of motional frequencies that create fluctuations in the local magnetic field due to the brownian motions of the molecule. These local fluctuations in

the magnetic field induce nuclear spin transitions that restore the system to equilibrium. The power spectral density function for an isotropic molecule can be described using the Lipari-Szabo model-free approach [10,11]:

$$J(\omega) = \frac{2}{5}\left\{\frac{S^2\tau_m}{1+\omega^2\tau_m^2} + \frac{(1-S^2)\tau}{1+\omega^2\tau^2}\right\}, \quad (4)$$

in which τ_m is the isotropic rotational correlation time of the molecule, $\tau = \tau_m\,\tau_e\,/(\tau_m + \tau_e)$ where τ_e describes internal ps motional processes and S^2 is the square of the generalized order parameter. The relaxation rates are insensitive to internal motions, τ_e, that are substantially faster than τ_m on the sub-ps time scale and motions significantly slower than τ_m that do not perturb the chemical shifts. This restricts the motional information derived by solution relaxation experiments to motions on the ns-ps timescale characterized by τ_m, τ_e, and S^2. Motions on the ms to μs timescale that perturb the chemical shift are characterized by $\Delta R_2(1/\tau_{cp})$.

Relaxation data can be analyzed by fitting to various motional models using the model-free formalism, allowing direct extraction of overall and internal correlation times and order parameters for each residue. The model-free formalism is most applicable to molecules with a clear overall molecular frame of reference. In disordered proteins, where an overall molecular frame of referenced is unclear, reduced spectral density mapping can be employed for analysis.[12–16]. This approach assumes that $dJ(\omega)/d\omega^2$ is linear between $J(\omega_H + \omega_x)$ and $J(\omega_H - \omega_x)$ and substitutes an average single value of $J(\epsilon\,\omega_H)$ for the linear combinations of $J(\omega_H + \omega_x)$, $J(\omega_H)$, and $J(\omega_H - \omega_x)$, shown in Equations 1–3, thereby reducing the number of variables in Equations 1–3 to J(0), $J(\omega_x)$, and $J(\epsilon\,\omega_H)$, and allowing direct calculation of the spectral densities based on the measured relaxation parameters. The spectral density, J(0), obtained using this approach contains contributions from the exchange term $\Delta R_2(1/\tau_{cp})$, if present. The reduced spectral mapping technique yields estimates of the magnitude of the spectral densities at particular frequencies that are directly related to the motional frequencies of the molecule.

Spectral density mapping for both ^{13}C and ^{15}N may be applied to proteins that display more complex dynamic behavior.[12–16]. One approach, which is applicable to both ^{13}C and ^{15}N relaxation,[13] assumes that $J(\omega) = a\omega^{-2} + b$ between $J(\omega_H - \omega_X)$ and $J(\omega_H + \omega_X)$ and substitutes a single value of $J(\epsilon\omega_H)$ for linear combinations of $J(\omega_H + \omega_X)$, $J(\omega_H)$, and $J(\omega_H - \omega_X)$ shown in Equations 5–7, to give:

$$R_1 = (d^2/4)[3J(\omega_X) + 7J(\varepsilon_2\omega_H)] + c^2J(\omega_X) \quad (5)$$

$$R_2 = (d^2/8)[4J(0) + 3J(\omega_X) + 13J(\varepsilon_3\omega_H)] + (c^2/6) \cdot [4J(0) + 3J(\omega_X)] + \Delta R_2(1/\tau_{cp}) \quad (6)$$

$$NOE = 1 - (d^2/4R_1)[\gamma H/\gamma X]5J(\varepsilon_1\omega_H), \quad (7)$$

in which ϵ_1, ϵ_2, and ϵ_3 are constants that approximate the linear combinations of $J(\omega_H + \omega_X)$, $J(\omega_H)$, and $J(\omega_H - \omega_X)$. For ^{15}N the values are $\epsilon_1 = 0.87$, $\epsilon_2 = 0.92$, and $\epsilon_3 = 0.96$; for ^{13}C the values are $\epsilon_1 = 1.56$, $\epsilon_2 = 1.12$, and $\epsilon_3 = 1.06$. The values of the high-frequency spectral densities may best be obtained using data collected at multiple magnetic field strengths allowing direct measurement of the slope defining $J(\omega_H + \omega_X)$, $J(\omega_H)$, and $J(\omega_H - \omega_X)$. In practice this is accomplished by measuring the field dependence of the cross-relaxation rate constants, σ_{XH}, calculated from measured R_1 and NOE data as shown:

$$\sigma_{XH} = R_1(NOE - 1)\gamma_X/\gamma_H. \quad (8)$$

The cross-relaxation rates constants are then related to the spectral densities by

$$\sigma_{XH} = -(d^2/4)5J(\varepsilon_1\omega_H). \quad (9)$$

The cross-relaxation rates at different Bo fields are then plotted versus Bo^{-2} and the line fitted to this function is used to estimate additional values of $J(\omega)$ needed for spectral density mapping. Alternatively the $J(\epsilon_1\omega_H)$ may be approximated using a first-order Taylor series expansion as described by Farrow et al.[13] The ability to extract motional information without invoking specific models makes the spectral density mapping approach particularly attractive for the analysis of disordered and partially folded systems.

Equilibrium Protein Folding of α2D

α_2D is a de novo design protein developed as a test for the principles of protein design. The protein consists of 36 residues that form a helix-turn-helix motif that dimerizes to forming a four-helix bundle, in a bisecting U motif (shown in Figure 1).[17] Prior studies have shown that the protein bears many of the hallmarks of native proteins, adopting a single unique conformation with defined core sidechain interactions and displays

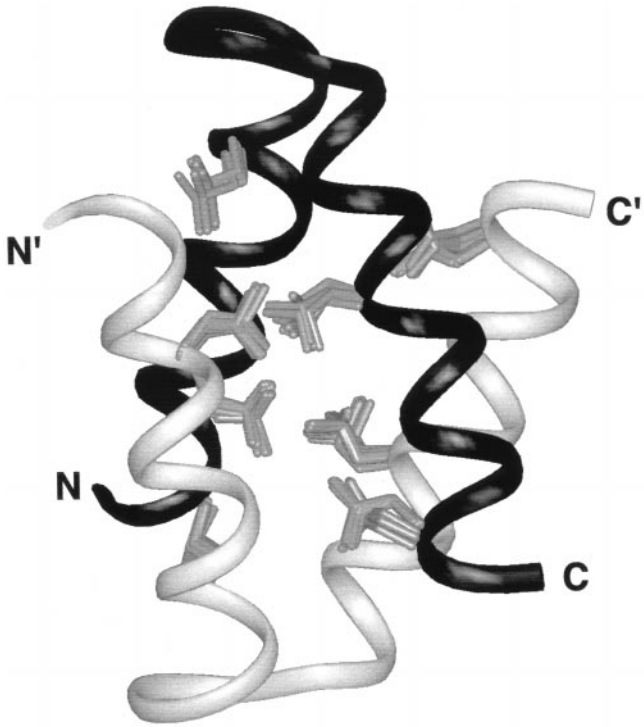

Figure 1. Structure of α_2D. The C^α backbone of α_2D is shown as a solid tube; the leucine side chains are shown as the superposition of the conformations observed in the ten lowest energy NMR solution structures of α_2D. The figure was drawn from the coordinates of PDB file 1qp6 using InsightII (MSI Research, San Diego, CA).

cooperative folding–unfolding transitions.[18] To assess more fully whether the α_2D peptide resembles native proteins, four leucine resonances, 6, 13, 25, and 32, were synthetically $^{13}C^{\alpha}$-labeled, providing probes of the hydrophobic core to investigate the backbone conformational dynamics.[19]

Relaxation rate constants were recorded at multiple static magnetic field strengths to probe ps to ns and μs to ms time scale dynamics and assess whether chemical exchange effects are present. The presence of exchange was assessed using the field dependence of the parameter, Γ, described by Phan et al. given below:[20]

$$\Gamma = (d^2/2)J(0) + (2\gamma_C^2\Delta\sigma^2 J(0)/9 + \Theta_{ex})B_0^2 \qquad (10)$$

where Θ_{ex} is the field-dependent chemical exchange term. Γ is linearly dependent on J(0) and the slope is a function of the chemical shift anisotropy and the chemical exchange term Θ_{ex}. In the absence of exchange effects the field dependence of the data is dominated solely by the chemical shift anisotropy term that causes a gradual increase in the parameter, Γ, as a function of increasing field strength. The presence of chemical exchange, Θ_{ex}, significantly increase the field dependence of Γ, making apparent the presence of chemical exchange effects. Figure 2 shows the dependence of the parameter Γ for the labeled $^{13}C^{\alpha}$ resonances of α_2D as a function of the B^2o field. The dashed line corresponds to the calculated field dependence in the absence of chemical exchange for $^{13}C^{\alpha}$, the slight increase in Γ with the field is due entirely to chemical shift anisotropy effects. The solid lines in Figure 2 correspond to the experimentally observed field dependence. The observed difference between the two lines indicate that significant chemical exchange effects are present in α_2D. Since α_2D is a dimer, two distinct mechanism were possible for generating these chemical exchange effects: conformational interconversion within the dimeric molecule and monomer–dimer exchange.

The nature of the chemical exchange event in α_2D was established by measuring the relaxation rates as a function of protein concentration using the relaxation-compensated CPMG experiment developed by Loria et al.[21] The relaxation-compensated CPMG experiment averages inphase and antiphase relaxation rates, allowing the relaxation delay, τ_{cp} , between 180° pulses to be significantly increased, thereby probing a broader range of exchange times. During short τ_{cp}, chemical exchange is minimized or entirely quenched, while longer τ_{cp} delays allow the effects of chemical exchange to manifest. Figure 3 shows the α_2D concentration dependence of the relaxation rates at short and long τ_{cp} relaxation delays using the compensated CPMG experiment. In a nonexchanging system, short and long τ_{cp} relaxation delays yield equivalent decay rates. α_2D shows a pronounced difference in the two rates, indicating the presence of chemical exchange. If the exchange effects arise from conformational interconversion of the leucine residues within the dimer, then the exchange effects will be independent of concentration. The divergence of the two relaxation rates as a function of concentration demon-

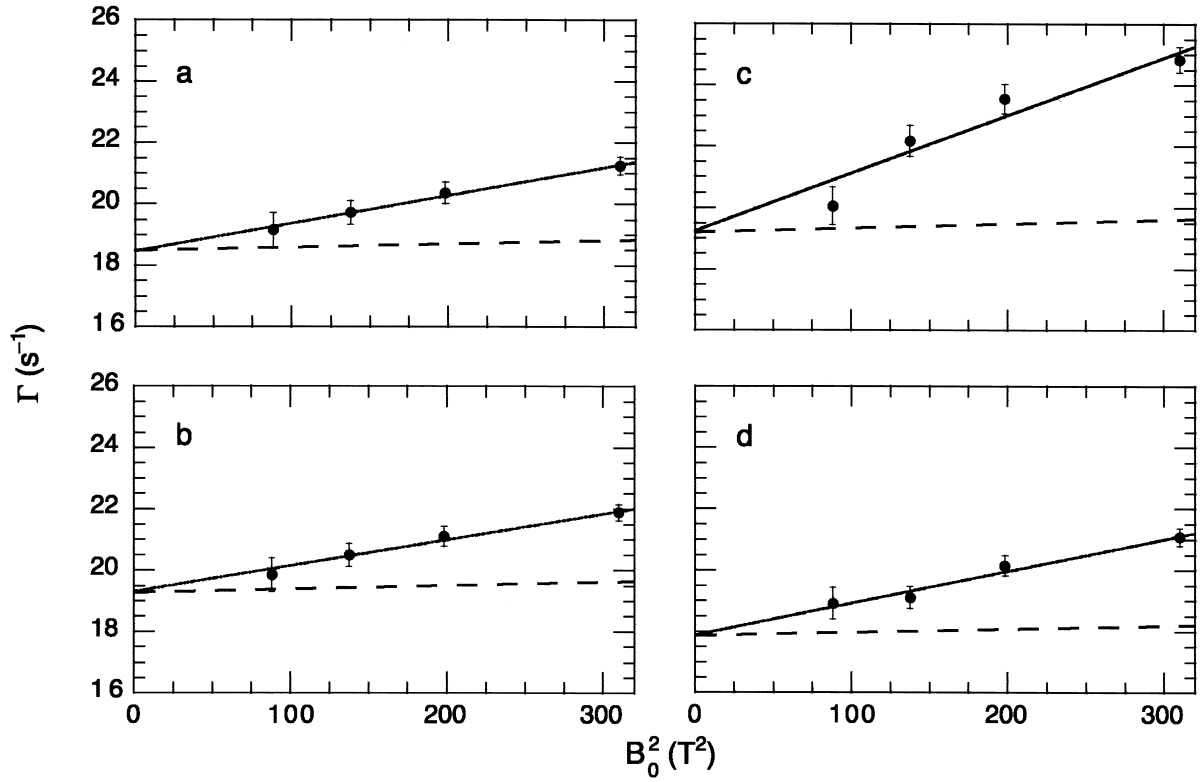

Figure 2. Chemical exchange contributions to spin relaxation in α_2D. Experimental values of Γ calculated using Equation 8 are plotted versus B_0^2 for (a) Leu 6, (b) Leu 13, (c) Leu 25, and (d) Leu 32. The solid lines are linear least-squares fits to the experimental data. The y*-intercepts are proportional to* J*(0) and the slopes depend on both the magnitude of the $^{13}C^{\alpha}$ CSA and on chemical exchange contributions to* R_2*. The dashed lines show the field dependence of Γ predicted in the absence of chemical exchange linebroadening.*

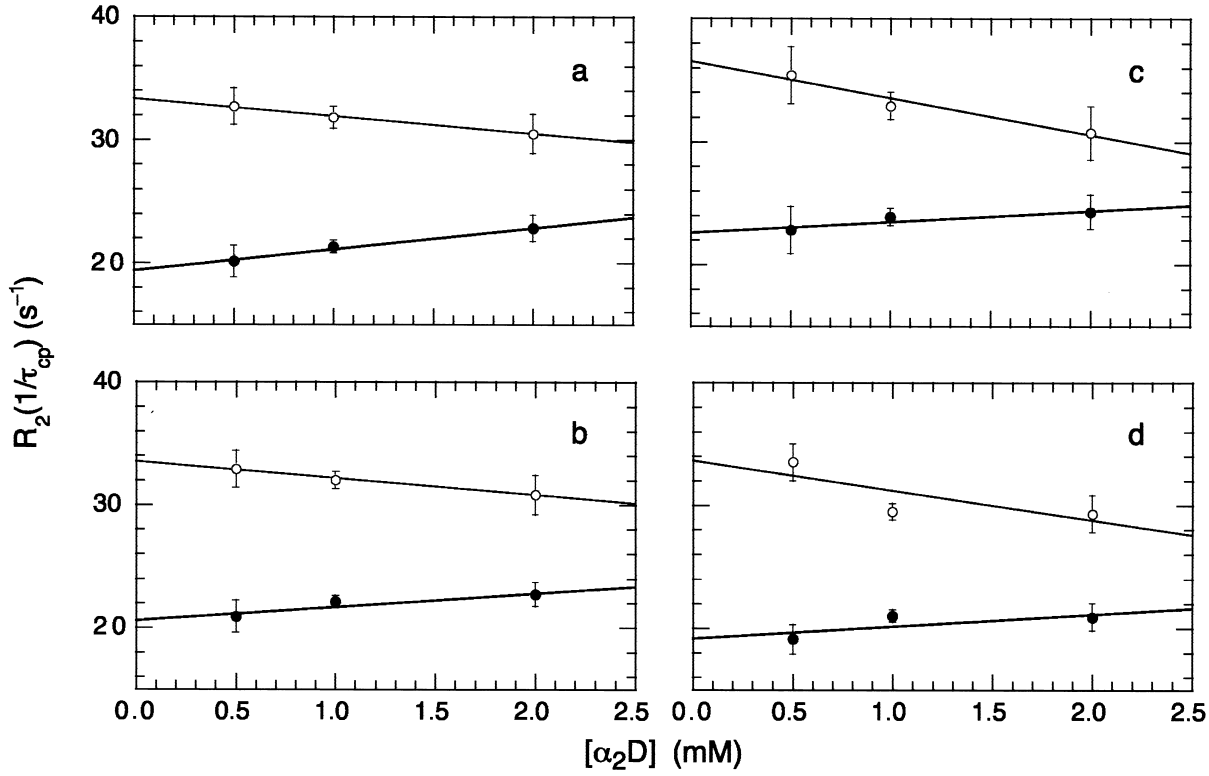

Figure 3. The folding equilibrium causes chemical exchange in α_2D. Values of $R_2(1/\tau_{cp})$ for (●) τ_{cp} = 0.5 ms and (○) τ_{cp} = 10.0 ms are plotted versus the total monomer concentration of α_2D for (a) Leu 6, (b) Leu 13, (c) Leu 25, and (d) Leu 32. Values of $R_2(1/\tau_{cp})$ at τ_{cp} = 10.0 ms for 2.0 mM α_2D were obtained by extrapolating the relaxation dispersion curves measured for τ_{cp} values ranging from 6.7 ms to 0.5 ms (data not shown). The decreased chemical exchange linebroadening at higher protein concentrations identifies the folding equilibrium for α_2D to be the mechanism for exchange linebroadening.

strates that the mechanism of exchange is due to a concentration dependent shift in the monmer–dimer equilibrium.

Once the mechanism of exchange is established, details about the kinetic rates of exchange and the chemical shift differences between the exchanging sites can be obtained. For chemical exchange between folded dimer and unfolded or partially folded monomer of α_2D, a two-site chemical exchange reaction is considered:

$$\mathrm{D} \underset{k_{-1}}{\overset{k_1}{\rightleftharpoons}} 2\mathrm{M} \tag{11}$$

in which [D], is the concentration of dimer and [M] is the concentration of monomer. The equilibrium disassociation constant for the exchange reaction $K_d = k_1/k_{-1}$, where k_1 is the forward first order kinetic rate constant (off-rate), and k_{-1} is the reverse second-order kinetic rate constant (on-rate). At equilibrium, the fraction of monomeric α_2D molecules is p_M = [M]/([M]+2[D]) and the fraction of α_2D molecules in dimers is $p_D = 1 - p_M$. Based on prior analytical ultracentrifugation studies the monomer population, p_M is known to be small under the conditions used for NMR studies.

A general expression for the transverse relaxation rate constant for exchange between two states, $R_2(1/\tau_{cp})$, is given by:[22–24]

$$R_2(1/\tau_{cp}) = \frac{1}{2}\left(R_M + R_D + k_{ex} - \frac{1}{\tau_{cp}} \cosh^{-1}[D_+ \cosh(\eta_+) - D_- \cos(\eta_-)] \right) \tag{12}$$

in which,

$$k_{ex} = 2[M]k_{-1} + k_1 = k_1/p_M = 2[M]k_{-1}/p_D \tag{13}$$

$$D_\pm = \frac{1}{2}\left[\pm 1 + \frac{\psi + 2\Delta\omega^2}{(\psi^2 + \zeta^2)^{1/2}} \right] \tag{14}$$

$$\eta_\pm = \frac{\tau_{cp}}{\sqrt{2}} [\pm \psi + (\psi^2 + \zeta^2)^{1/2}]^{1/2} \tag{15}$$

$$\psi = (R_D - R_M - p_D k_{ex} + p_M k_{ex})^2 - \Delta\omega^2 + 4 p_D p_M k_{ex}^2 \tag{16}$$

$$\zeta = 2\Delta\omega(R_D - R_M - p_D k_{ex} + p_M k_{ex}), \tag{17}$$

where τ_{cp} is the delay between 180° pulses in the CPMG pulse train. The frequency difference between the chemical shifts of the two sites is $\Delta\omega = \left| \omega_M - \omega_D \right|$. The transverse relaxation rate constants for the nonexchanging monomers and dimers are R_M and R_D, respectively. For the relaxation-compensated CPMG experiments, R_M and R_D correspond to the average relaxation rates for in-phase and antiphase coherences[21]. The

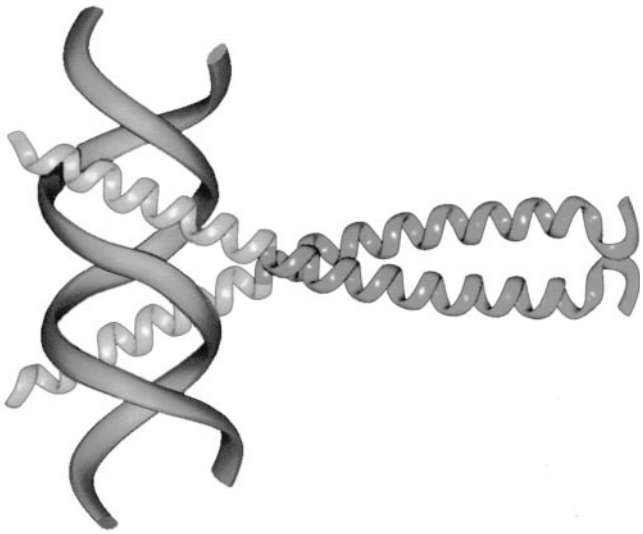

Figure 4. Structure and sequence of GCN4-58. (top) Ribbon diagram of the GCN4 bZip DNA binding domain and dimerization domain complexed with DNA. The figure was drawn from the coordinates of PBD file 1ysa using Insight II (MSI Research, San Diego, CA).

relaxation rates $R_2(1/\tau_{cp})$ are collected as a function of the delay τ_{cp}, generating a relaxation curve influenced only by the presence of chemical exchange shown for α_2D in Figure 4.

One factor that complicates the extraction and analysis of the chemical exchange parameters is the timescale of the exchange regime. When the chemical exchange regime is slow ($k_{ex}/\Delta\omega < 1$), the contribution of chemical exchange to $R_2(1/\tau_{cp})$ vanishes during small values of τ_{cp}. However, when the exchange regime is fast ($k_{ex}/\Delta\omega > 1$), the chemical exchange contributes to $R_2(1/\tau_{cp})$ for the small τ_{cp} delay times. In α_2D, establishing the exchange regime was problematic, since the small population of monomer at millimolar concentrations would be difficult to observe in the slow-exchange regime and invisible under fast-exchange conditions. Additionally, the relaxation compensated CPMG data collected at a single field could be adequately fit to either the fast- or slow-exchange regimes for α_2D.

Millet et al.[24] recently developed a method for establishing whether exchange processes occur on a fast or slow timescale. They have defined a parameter, α, that characterizes the static magnetic-field dependence of R_{ex}, which distinguishes the exchange regime:

$$\alpha = \left(\frac{B_{02} - B_{01}}{B_{02} + B_{01}}\right)\left(\frac{R_{ex2} - R_{ex1}}{R_{ex2} + R_{ex1}}\right) \qquad (18)$$

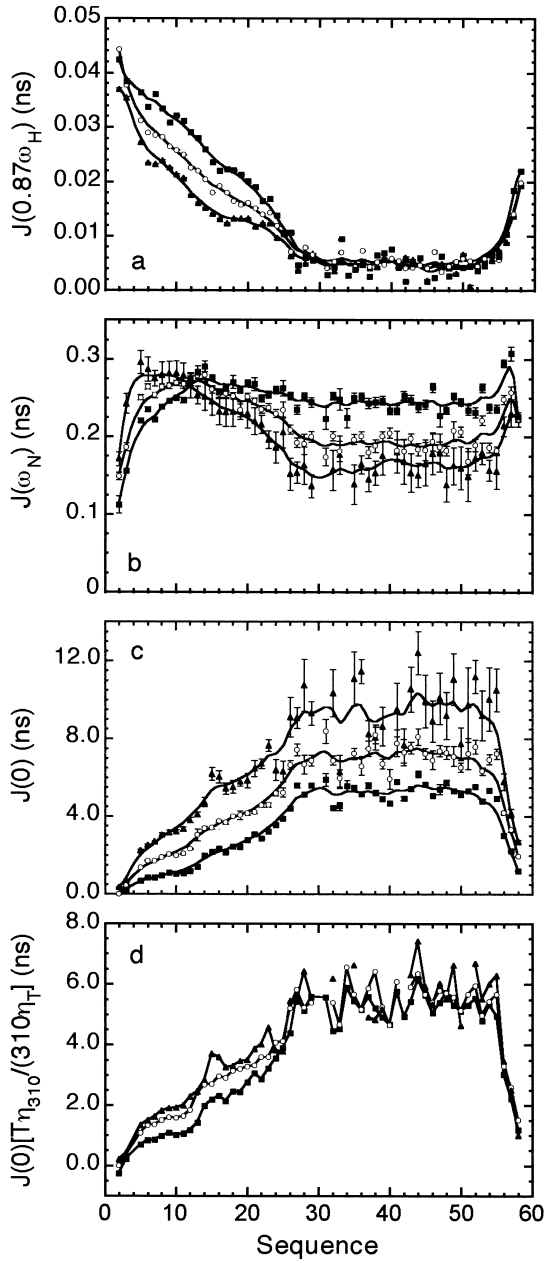

Figure 5. Reduced spectral densities as a function of sequence for GCN4-58. Reduced spectral density functions (a) $J(0.87\omega_H)$, (b) $J(\omega_N)$, and (c) $J(0)$ for GCN4-58 at (▲) 290, (○) 300 K, and (■) 310 K. (d) Values of $J(0)(\eta/T)/(\eta_{310}/310)$ are plotted to normalize for differences in temperature and viscosity relative to 310 K.

Table 2. Chemical Exchange Parameters for α_2D

Residue	R_2^0 (s^{-1})	p_M	$\Delta\omega$ (ppm)	k_{ex} (s^{-1})
Leu 6	22.6 ± 0.5	0.038 ± 0.006	0.89 ± 0.11	510 ± 170
Leu 13	22.6 ± 0.4	0.028 ± 0.007	1.12 ± 0.15	580 ± 220
Leu 25	25.0 ± 0.6	0.019 ± 0.002	1.31 ± 0.17	940 ± 310
Leu 32	21.7 ± 0.5	0.024 ± 0.004	1.16 ± 0.13	540 ± 160

in which R_{ex1} and R_{ex2} are the exchange contributions obtained from Equation 12 for data recorded at two different magnetic field strengths B_{01} and B_{02}. The parameter α is limited to values between 0 and 2 for $p_D > 0.7$; for exchange that is slow ($k_{ex}/\Delta\omega < 1$) on the chemical shift time scale, values of $\alpha < 1$ are obtained; and for exchange that is fast ($k_{ex}/\Delta\omega > 1$) on the chemical shift time scale, values of $\alpha > 1$ are obtained. Acquisition of NMR relaxation data at a B_{01}=11.7 T and B_{02}= 14.1 T yielded α values between 0.44 to 0.82 for α_2D, dem-

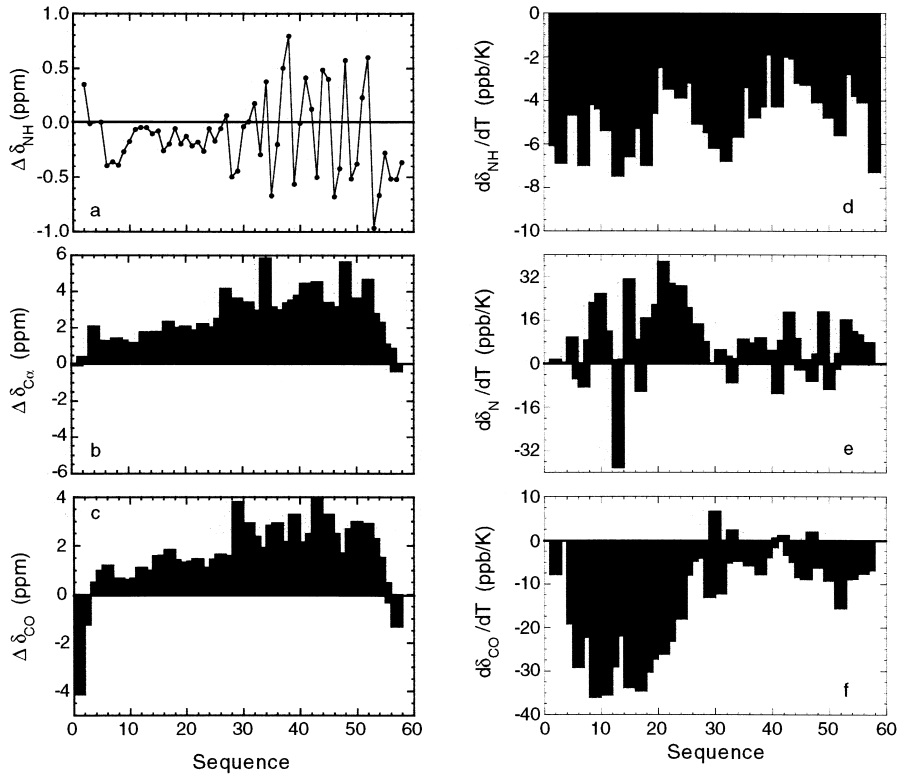

Figure 6. Chemical shift deviations from random coil values and the temperature-dependent chemical shifts of GCN4-58.The right column displays the chemical shift deviation for (a) ^{1}H, (b) $^{13}C^{\alpha}$, and (c) ^{13}CO. The left column displays the chemical shift temperature dependence of the (d) $^{1}H^{N}$, (e) ^{15}N, and (f) ^{13}CO. The chemical shift deviations from random coil values and the temperature dependence of the chemical shifts indicate the presence of nascent helical structure in the basic region of GCN4.

onstrating that the monomer–dimer exchange process occurs in the slow regime.

The $R_2(1/\tau_{cp})$ dispersion curves acquired on α_2D at static magnetic fields of 11.7 and 14.1 T were fit simultaneously to Equation 12, allowing extraction of the independent fitting parameters $R_2^0 = p_M R_M + p_D R_D$, $p_M p_D$, $\Delta\omega$, and k_{ex}. Table 2 shows the chemical exchange parameters obtained from the fit for α_2D. The average results for $p_M = 0.028 \pm 0.003$ and $k_{ex} = 540 \pm 100\ s^{-1}$ for Leu 6, Leu 13, and Leu 32 yield estimates of $K_d = 2.7 \pm 0.6\ \mu$M, $k_1 = 15 \pm 3\ s^{-1}$, and $k_{-1} = (4.7 \pm 0.9) \times 10^6\ M^{-1}\ s^{-1}$.[19] The value of K_d is in basic agreement with prior estimates of $K_d = 7 \pm 3\ \mu$M obtained using ultracentrifugation.

Residual Structure and Entropy in the Basic Leucine Zipper of GCN4.

The bZip domain of the yeast transcription factor GCN4 consists of a C-terminal leucine zipper and an N-terminal basic DNA-binding region that achieves a stable structure only upon binding DNA (Figure 4).[25] The DNA-bound and -unbound conformation of GCN4 has been studied by numerous groups with an eye toward examining the structured regions.[26–30]. However, a similar level of scrutiny has not been expended upon understanding the conformational dynamics of the unbound state of GCN4, particularly the basic DNA-binding region. Yet the conformational dynamics and preexisting structural propensities within the basic region have profound consequences on the thermodynamics and recognition involved in DNA-binding. The NMR assignments and ^{15}N relaxation studies of GCN4-58 were undertaken to characterize the basic DNA-binding region of the free peptide in solution and to gain insight into the structural propensities and binding energetics of the DNA binding site.[31]

GCN4-58 is composed of a stable leucine zipper domain and a flexible basic region making model-free analysis problematic; therefore, the ^{15}N relaxation experiments were analyzed using spectral density mapping, with results shown in Figure 5.[31] All the spectral density plots display sharp contrasts between the N-terminal basic region of the protein, consisting of residues 1 through 24, and the dimerization region, which consists of a stable leucine zipper consisting of residues 25 through 54. The J(0), J(ω_N) and J($0.87\omega_H$) rates are fairly constant across the coiled coil. Proceeding from the N-terminus the J(0) values (Figure 5c) increase and J(ω_H) values (Figure 5a) decrease, corresponding to an increase in slower motions in the backbone resonances as they approach the coiled-coil region. The gradual nature of the transition over 20 residues suggests that significant residual structure in the basic region is present.

Confirmation that residual structure exists in the basic region is observed in the temperature dependence of the J(0) data, which is directly related to the overall correlation time of the molecule. In static structural states the relaxation data scales

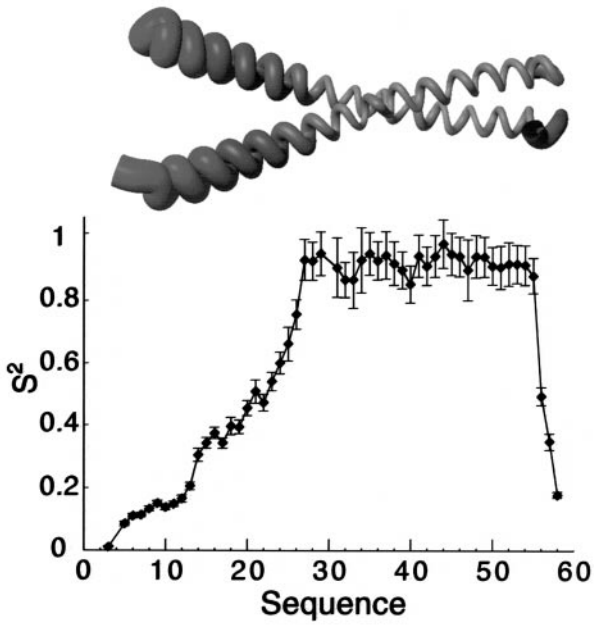

Figure 7. Amplitudes of intramolecular motions in GCN4-58. Shown above is the worm display of GCN4-58. The width and color of the backbone tube are proportional to the inverse of $J(0.87\omega_H)$. Values of $J(0.87\omega_H)$ were interpolated for residues for which relaxation data was not be obtained. The figure was drawn using MOLMOL. Shown below in register with the worm display, a graph of the approximate order parameter S^2 at 310 K derived from spectral density mapping using Equation 18 is graphed versus amino acid sequence.

according to the Stoke-Einstein equation as a function of the η/T where η is the intrinsic viscosity and T is the temperature in kelvin. In cases where interconverting conformers are shifting their equilibrium population, the relaxation data no longer scale with η/T but display deviations. After corrections for differences in temperature and viscosity effects, the normalized J(0) values, shown in Figure 5d, display distinctive differences only in the disordered basic region of the protein, indicating temperature-dependent conformational change.

The temperature dependence of the chemical shifts (Figure 6) in conjunction with the temperature dependence of the NMR relaxation parameters confirms both the formation and identity of secondary structure in the basic region.[31–33] The chemical shifts $^{13}C^{\alpha}$ and ^{13}CO are good indicators of secondary structure, while the temperature dependence of the chemical shifts is often strong in regions undergoing structural interconversion.[9,34,35] Whereas in fully structured regions and in random-coil regions the temperature dependence of these resonances are generally small.[34] In GCN4-58 the deviations in the regions mapped by the both temperature-dependent NMR dynamics measurements and temperature-dependent chemical shifts strongly indicate the presence of nascent helical structure; the direction of the chemical shift change indicates helical formation as the temperature is lowered.

Further information about the basic region may be obtained by analyzing the order parameters, S^2, describing the degree of correlation to the overall molecular tumbling. For well-ordered sites in a macromolecule a local overall rotational correlation time, τ_M, is obtained from the spectral density functions as

$$\tau_M = \omega_M^{-1}\left(\frac{J(0) - J(\omega_N)}{J(\omega_N)}\right)^{1/2}. \qquad (19)$$

Once a value of τ_M has been determined, the amplitude of intramolecular motion of the N—H bond vector in a molecular reference frame is approximated by[15]

$$S^2 = \frac{5(J(0) - J(\omega_N))(1 - \omega_N^2\tau_M^2)}{2\omega_N^2\tau_M^3}. \qquad (20)$$

The parameter S^2 of Equation 20 is an approximation to the square of the generalized order parameter that appears in the model-free spectral density function.[11] Provided that τ_M can be estimated, Equation 20 provides a good approximation to S^2 for effective internal correlation times up to 1 ns. Figure 7 displays the values of S^2 obtained for GCN4 using the spectral density mapping approach, with a worm diagram (top of figure) lined up in register to graphically depict the changes in S^2.

Estimates of S^2 obtained using either the model-free or spectral density mapping approach allow estimation of the extent to which the reduction of conformational space accessible to partially folded or disordered proteins contributes to the thermodynamics of protein folding. This was first demonstrated by Akke et. al. for estimating the configurational backbone entropy from changes in order parameter in the calcium binding protein calmodulin in both the presence and absence of calcium.[36] For very low-order parameters, which are generally observed in disordered proteins, the use of the linearized approximation to the partition function and a specific model potential must be assumed.[36,37] The change in conformational entropy of the peptide backbone going from a disordered to an ordered state is given by[36]

$$\Delta S = -k_B \sum_i \ln\left\{\frac{3 - (1 + 8S_{b,i})^{1/2}}{3 - (1 + 8S_{f,i})^{1/2}}\right\}, \qquad (21)$$

in which k_B is Boltzmann's constant, $S^2_{b,i}$ is the value of S^2 in a bound or folded state, and $S^2_{f,i}$ is the value of S^2 derived from Equation 20 for a disordered protein or peptide. The index refers to the *i*th spin in the polypeptide. This equation allows estimation of the backbone configurational entropy for changes in S^2 due to ligand binding, folding, and other structural perturbations that affect the motions of proteins. By making the assumption that the DNA-bound conformation of GCN4 adopts a stable backbone conformation, the values of S^2 can be fixed to values commonly observed in folded proteins, $S^2_f = 0.86$. Applying Equation 21 to the data for S^2 in Figure 7 yields $\Delta S = -0.6$ kJ K^{-1} mol^{-1}.[31]

Extant data for the estimation of ΔS_{conf} for GCN4 gives a total $\Delta S_{conf} = -1.2$ kJ K^{-1} mol^{-1} is based on calorimetric data.[38] Monte Carlo and MD simulations and examinations of the distribution of side chain rotamers in protein structures indicate that ~40–45% of the total conformational entropy loss associated with folding a random peptide arises from the peptide backbone chain entropy[37,39]; the remainder arises from ordering of the side chains.[40–42]. Therefore, the fraction of the experimental ΔS_{conf} predicted to arise from backbone conformational effects is approximately -0.5 kJ K^{-1} mol^{-1}. The agreement between independent measurements of the backbone conformational entropy of binding by NMR spin relax-

ation and by theoretical analysis of calorimetric data implies that the approach has merit. This suggests that the backbone dynamics in the basic region measured by NMR spectroscopy accounts for a significant fraction of the conformational entropy determined calorimetrically. Consequently, NMR studies will permit dissection of the entropic contributions to DNA recognition by bZip and protein binding events at an atomic level.

CONCLUSIONS

The variety of relaxation methods for examining disorder in protein conformations continues to grow. In recent years notable advances have occurred in NMR relaxation data collection and analysis that allow access to motional regimes from the ms to ps time scales. Most notable are the expansion of methodologies for obtaining conformational exchange rates and for the estimation backbone configurational entropy. The recent development of novel NMR relaxation methods promises to offer additional means of assessing dynamics at multiple locations throughout the entire protein providing,site-specific analysis of the equilibrium folding-unfolding kinetics of proteins. This expansion in relaxation methodology is coupled with the development of new pulse sequences and protein labeling techniques that are opening investigations to larger and more complex protein systems.

ACKNOWLEDGMENTS

We would like to thank Blake Hill, Christopher Kroenke, Patrick Loria, and Arthur G. Palmer for many helpful discussions. C.B. acknowledges financial support from the American Heart Association.

REFERENCES

1 Wright, P.E., Dyson, H.J. Intrinsically unstructured proteins: re-assessing the protein structure–function paradigm. *J. Mol. Biol.* 1999, **293**, 321–331
2 Sattler, M., Schleucher, J., Griesinger, C. Heteronuclear multidimensional NMR experiments for the structure determination of proteins in solution employing pulsed field gradients. *Prog. NMR Spectrosc.* 1999, **34**, 93–158
3 Palmer, A.G. Probing molecular motion by NMR. *Curr. Opin. Struct. Biol.* 1997, **7**, 732–737
4 Kay, L.E. Protein dynamics from NMR. *Nat. Struct. Biol.* 1998, **NMR Suppl.**, 513–517
5 Palmer, A.G., Bracken, C. Spin relaxation methods for characterizing picosecond-nanosecond and microsecond-millisecond motions in proteins. In: *NMR in Supramolecular Chemistry*. Pons, M., Ed., Kluwer Academic Publishers, Dordrecht. pp. 171–190, 1999
6 Abragam, A. *Principles of Nuclear Magnetism*. Clarendon Press, Oxford, 1961, pp. 264–353
7 Farrow, N.A., Muhandiram, R., Singer, A.U., Pascal, S.M., Kay, C.M., Gish, G., Shoelson, S.E., Pawson, T., Forman-Kay, J.D., and Kay, L.E. Backbone dynamics of a free and a phosphopeptide-complexed Src homology 2 domain studied by ^{15}N NMR relaxation. *Biochemistry* 1994, **33**, 5984–6003
8 Skelton, N.J., Palmer, A.G., Akke, M., Kördel, J., Rance, M., and Chazin, W.J. Practical aspects of two-dimensional proton-detected ^{15}N spin relaxation measurements. *J. Magn. Reson. B* 1993, **102**,253–264
9 Spera, S., and Bax, A. Empirical correlation between protein backbone conformation and Cα and Cβ ^{13}C nuclear magnetic resonance chemical shifts. *J. Am. Chem. Soc.* 1991, **113**,5490–5492
10 Clore, G.M., Szabo, A., Bax, A., Kay, L.E., Driscoll, P.C., and Gronenborn, A.M. Deviations from the simple two-parameter model-free approach to the interpretation of nitrogen-15 nuclear magnetic relaxation of proteins. *J. Am. Chem. Soc.* 1982, **112**,4989–4991
11 Lipari, G., and Szabo, A. Model-free approach to the interpretation of nuclear magnetic resonance relaxation in macromolecules. 1. Theory and range of validity. *J. Am. Chem. Soc.* 1990, **104**, 4546–4559
12 Farrow, N.A., Zhang, O., Forman-Kay, J.D., and Kay, L.E. Characterization of the backbone dynamics of folded and denatured states of an SH3 domain. *Biochemistry* 1992, **36**, 2390–2402
13 Farrow, N.A., Zhang, O., Szabo, A., Torchia, D.A., and Kay, L.E. Spectral density function mapping using ^{15}N relaxation data exclusively. *J. Biomol. NMR* 1995, **6**, 153–162
14 Ishima, R., and Nagayama, K. Protein backbone dynamics revealed by quasi spectral density function analysis of amide N-15 nuclei. *Biochemistry* 1995, **34**, 3162–3171
15 Lefevre, J.F., Dayie, K.T., Peng, J.W., and Wagner, G. Internal mobility in the partially folded DNA binding and dimerization domains of GAL4: NMR analysis of the N-H spectral density functions. *Biochemistry* 1996, **35**, 2674–2686
16 Peng, J.W., and Wagner, G. Mapping spectral density functions using heteronuclear NMR relaxation measurements. *J. Magn. Reson.* 1997, **98**, 308–332
17 Hill, and B.R., Degrado, W.F. Solution structure of α_2D, a nativelike de novo designed protein. *J. Amer. Chem. Soc.* 1998, **120**, 1138–1145
18 Raleigh, D.P., Betz, S.F., and Degrado, W.F. A de novo designed protein mimics the native state of natural protein. *J. Amer. Chem. Soc.* 1995, **117**, 7558–7559
19 Hill, R.B., Bracken, C., DeGrado, W.F., and Palmer, A.G. Molecular Motions and Protein Folding: Characterization of the Backbone Dynamics and Folding Equilibrium of a2D using 13C NMR Spin Relaxation. *J. Amer. Chem. Soc.* 2000, **122**, 11610–11619
20 Phan, I.Q.H., Boyd, J., and Campbell, I.D. Dynamic studies of a fibronectin type I module pair at three frequencies: Anisotropic modelling and direct determination of conformational exchange. *J. Biomol. NMR* 1996, **8**, 369–378
21 Loria, J.P., Rance, M., and Palmer, A.G. A relaxation-compensated Carr-Purcell-Meiboom-Gill sequence for characterizing chemical exchange by NMR spectroscopy. *J. Amer. Chem. Soc.* 1999, **121**, 2331–2332
22 Davis, D.G., Perlman, M.E., and London, R.E. Direct measurements of the dissociation-rate constant for inhibitor-enzyme complexes via the $T_{1\rho}$ and T_2 (CPMG) methods. *J. Magn. Reson., Ser B* 1994, **104**, 266–275
23 Jen, J. Chemical exchange and NMR T_2 relaxation — the multisite case. *J. Magn. Reson.* 1978, **30**, 111–128
24 Millet, O., Loria, J.P., Kroenke, C.D., Pons, M., and Palmer, A.G. The static magnetic field dependence of chemical exchange linebroadening defines the NMR

chemical shift time scale. *J. Amer. Chem. Soc.* 2000, **122**, 2867–2877
25 Ellenberger, T.E., Brandl, C.J., Struhl, K., and Harrison, S.C. The GCN4 basic region leucine zipper binds DNA as a dimer of uninterrupted α-helices: crystal structure of the protein-DNA complex. *Cell* 2000, **71**, 1223–1237
26 Holtzer, M.E., Lovett, E.G., d'Avignon, D.A., and Holtzer, A. Thermal unfolding in a GCN4-like leucine zipper: 13C alpha chemical shifts in local unfolding curves. *Biophys. J.* 1990, **73**, 1031–1041
27 Saudek, V., Pasley, H.S., Gibson, T., Gausepohl, H., Frank, R., and Pastore, A. Solution structure of the basic region from the transcriptional activator GCN4. *Biochemistry* 1990, **30**, 1310–1317
28 Saudek, V., Pastore, A., Castiglione Morelli, M.A., Frank, R., Gausepohl, H., and Gibson, T. The solution structure of a leucine-zipper motif peptide. *Prot. Engineer.* 1991, **4**, 519–529
29 Saudek, V., Pastore, A., Morelli, M.A.C., Frank, R., Gauspohl, H., Gibson, T., Weih, F., and Roesch, P. Solution structure of the DNA-binding domain of the yeast transcription activator protein GCN4. *Protein Eng.* 1990, **30**, 1317–1323
30 Weiss, M.A. Thermal unfolding of a leucine zipper domain and its specific DNA complex: implications for scissor's grip recognition. *Biochemistry* 1990, **29**, 8020–8024
31 Bracken, C., Carr, P.A., Cavanagh, J., and Palmer, A.G. Temperature dependence of intramolecular dynamicsof the basic leucine zipper of GCN4: implications for the entropy of association with DNA. *J. Mol. Biol.* 1999, **285**, 2133–2146
32 O'Neil, K.T., Shuman, J.D., Ampe, C., and DeGrado, W.F. DNA-Induced Increase in the α-Helical Content of C/EBP and GCN4 1991, **37**, 9030–9034
33 Weiss, M.A., Ellenberger, T., Wobbe, C.R., Lee, J.P., Harrison, S.C., and Struhl, K. Folding transition in the DNA-binding domain of GCN4 on specific binding to DNA. *Nature* 1990, **347**, 575–578
34 Shalongo, W., Dugad, L., and Stellwagen, E. Analysis of the thermal transitions of a model helical peptide using ^{13}C NMR. *J. Am. Chem. Soc.* 1994, **116**, 2500–2507
35 Wishart, D.S., Bigam, C.G., Arne, H., Hodges, R.S., and Sykes, B.D. ^{1}H, ^{13}C, ^{15}N random coil NMR chemical shifts of the common amino acids. I. Investigation of nearest-neighbor errects. *J. Biomol. NMR* 1995, **5**, 67–81
36 Akke, M., Brüschweiler, R., and Palmer, A.G. NMR order parameters and free energy: An analytic approach and application to cooperative Ca^{2+} binding by calbindin D_{9k}. *J. Am. Chem. Soc.* 1993, **115**, 9832–9833
37 Yang, D., Kay, L.E. Contributions to conformational entropy arising from bond vector fluctuations measured from NMR-derived order parameters: Application to protein folding. *J. Mol. Biol.* 1996, **263**, 369–382
38 Berger, C., Ilian, J., and Bosshard, H.R. Coupled folding and site-specific binding of the GCN4-bZIP transcription factor to the AP-1 and ATF/CREB DNA sites studied by microcalorimetry. *Biochemistry* 1996, **35**, 14984–14991
39 Dill, K.A., Alonso, D.O.V., and Hutchinson, K. Thermal stabilities of globular proteins. *Biochemistry* 1989, **28**, 5439
40 Creamer, T.P., and Rose, G.D. Side-chain entropy opposes alpha-helix formation but rationalizes experimentally determined helix-forming propensities. *Proc. Natl. Acad. Sci. U.S.A.* 1992, **89**, 5937–5941
41 Pickett, S.D., and Sternberg, M.J.E. Empirical scale of side-chain conformational entropy in protein-folding. *J. Mol. Biol.* 1993, **231**, 825–839
42 Spolar, R.S., and Record, M.T. Coupling of local folding to site-specific binding of proteins to DNA. *Science* 1994, **263**, 777–784